

Adiabatic compression of quadratic temporal solitons in aperiodic quasi-phase-matching gratings

Xianglong Zeng, Satoshi Ashihara, Nobuhide Fujioka, Tsutomu Shimura, and Kazuo Kuroda

Institute of Industrial Science, The University of Tokyo, Komaba 4-6-1, Meguro-ku, Tokyo, 153-8505, Japan

Abstract: We numerically show that it is possible to achieve adiabatic compression of femtosecond quadratic solitons in aperiodically poled lithium niobate device. Two-colored solitons of the fundamental wavelength of 1560 nm can be adiabatically shaped by using group-velocity matching schemes available in quasi-phase-matching (QPM) devices. We investigate the performance of the adiabatic compression based on two different group-velocity matching schemes: type-I (e: $o + o$) collinear QPM geometry and type-0 (e: $e + e$) non-collinear QPM geometry. Two-colored temporal solitons with pulse duration of 35 fs are generated without visible pedestals from 100-fs fundamental pulse. We also show that walking solitons with shorter pulse durations are adiabatically excited under small group-velocity mismatch condition. The walking solitons experience deceleration or acceleration during compression, depending on the sign of the group-velocity-mismatch. The demonstrated adiabatic pulse shaping is useful for generation of shorter pulses with clean temporal profiles, efficient femtosecond second harmonic generation and group-velocity control.

©2005 Optical Society of America

OCIS codes: (190.5530) Pulse propagation and solitons; (190.7110) Ultrafast nonlinear optics; (320.5520) Pulse compression.

References and links

1. C. Menyuk, R. Schiek, and L. Torner, "Solitary waves due to $\chi^{(2)}:\chi^{(2)}$ cascading," J. Opt. Soc. Am. B **11**, 2434-2443 (1994).
2. G. I. Stegeman, D. J. Hagan, and L. Torner, " $\chi^{(2)}$ Cascading phenomena and their applications to all-optical signal processing, mode-locking, pulse compression and solitons," J. Opt. Quant. Electron. **28**, 1691-1740 (1996).
3. L. Torner and A. Barthelemy, "Quadratic solitons: recent developments," IEEE J. Quantum Electron. **39**, 22-30 (2003).
4. A. V. Buryak, P. Di Trapani, D. Skryabin, and S. Trillo, "Optical solitons due to quadratic nonlinearities: from basic physics to futuristic applications," Phys. Rep. **370**, 63-235 (2002).
5. A. V. Buryak and Y. S. Kivshar, "Spatial optical solitons governed by quadratic nonlinearity," Opt. Lett. **19**, 1612-1615(1994).
6. L. Torner, "Stationary solitary waves with second-order nonlinearities," Opt. Commun. **114**, 136-140 (1995).
7. W. E. Torruellas, Z. Wang, D. J. Hagan, E. W. VanStryland, G. I. Stegeman, L. Torner, and C. R. Menyuk, "Observation of two-dimensional Spatial Solitary Waves in a Quadratic Medium," Phys. Rev. Lett. **74**, 5036-5039 (1995).
8. R. Malendevich, L. Jankovic, S. Polyakov, R. Fuerst, G. Stegeman, C. Bosshard, and P. Gunter, "Two-dimensional type I quadratic spatial solitons in KNbO₃ near noncritical phase matching," Opt. Lett. **27**, 631-633 (2002).
9. B. Bourliaguet, V. Couderc, A. Barthelemy, G. Ross, P. Smith, D. Hanna, and C. De Angelis, "Observation of quadratic spatial solitons in periodically poled lithium niobate," Opt. Lett. **24**, 1410-1412 (1999).
10. H. Kim, L. Jankovic, G. Stegeman, S. Carrasco, L. Torner, D. Eger, and M. Katz, "Quadratic spatial solitons in periodically poled KTiOPO₄," Opt. Lett. **28**, 640-642 (2003).
11. L. Torner, C. Clausen, and M. Fejer, "Adiabatic shaping of quadratic solitons," Opt. Lett. **23**, 903-905 (1998).

12. S. Carrasco, J. Torres, L. Torner, and R. Schiek, "Engineerable generation of quadratic solitons in synthetic phase matching," *Opt. Lett.* **25**, 1273-1275 (2000).
13. R. Schiek, R. Iwanow, T. Pertsch, G. I. Stegeman, G. Schreiber, and W. Sohler, "One-dimensional spatial soliton families in optimally engineered quasi-phase-matched lithium niobate waveguides," *Opt. Lett.* **29**, 596-598 (2004).
14. F. W. Wise, L. Qian, and X. Liu, "Applications of Cascaded Quadratic Nonlinearities to Femtosecond Pulse Generation," *J. Nonlinear Opt. Phys. Mater.* **11**, 317-338 (2002).
15. X. Liu, L. J. Qian, and F. Wise, "High-energy pulse compression by use of negative phase shifts produced by the cascade $\chi^{(2)}:\chi^{(2)}$ nonlinearity," *Opt. Lett.* **24**, 1777-1779 (1999).
16. S. Ashihara, J. Nishina, T. Shimura, and K. Kuroda, "Soliton compression of femtosecond pulses in quadratic media," *J. Opt. Soc. Am. B* **19**, 2505-2510 (2002).
17. K. Beckwitt, F. Ilday, and F. Wise, "Frequency shifting with local nonlinearity management in nonuniformly poled quadratic nonlinear materials," *Opt. Lett.* **29**, 763-765 (2004).
18. J. Moses and F. W. Wise, "Soliton compression in quadratic media: high-energy few-cycle pulses with a frequency-doubling crystal," *Opt. Lett.* **31**, 1881-1883 (2006).
19. S. Ashihara, T. Shimura, K. Kuroda, Nan Ei Yu, S. Kurimura, K. Kitamura, Myoungsik Cha, and Takunori Taira, "Optical pulse compression using cascaded quadratic nonlinearities in periodically poled lithium niobate," *Appl. Phys. Lett.* **84**, 1055-1057 (2004).
20. N. E. Yu, J. H. Ro, M. Cha, S. Kurimura, and T. Taira, "Broadband quasi-phase-matched second-harmonic generation in MgO-doped periodically poled LiNbO₃ at the communications band," *Opt. Lett.* **27**, 1046-1048 (2002).
21. S. Ashihara, T. Shimura, and K. Kuroda, "Group-velocity matched second-harmonic generation in tilted quasi-phase-matched gratings," *J. Opt. Soc. Am. B* **20**, 853-856 (2003).
22. S. Chernikov and P. Mamyshev, "Femtosecond soliton propagation in fibers with slowly decreasing dispersion," *J. Opt. Soc. Am. B* **8**, 1633-1641 (1991).
23. L. Torner and G. Stegeman, "Soliton evolution in quasi-phase-matched second-harmonic generation," *J. Opt. Soc. Am. B* **14**, 3127-3133 (1997).
24. G. P. Agrawal, *Nonlinear Fiber Optics*, 3rd Edition, (Academic Press).
25. D. Zelmon, D. Small, and D. Jundt, "Infrared corrected Sellmeier coefficients for congruently grown lithium niobate and 5 mol. magnesium oxide doped lithium niobate," *J. Opt. Soc. Am. B* **14**, 3319-3322 (1997).
26. G. Valiulis, A. Dubietis, R. Danielius, D. Caironi, A. Visconti, and P. Di Trapani, "Temporal solitons in $\chi^{(2)}$ materials with tilted pulses," *J. Opt. Soc. Am. B* **16**, 722-731 (1999).
27. E. Martinez, "Achromatic phase matching for second harmonic generation of femtosecond pulses," *IEEE J. Quantum Electron.* **25**, 2464-2468 (1989).
28. P. Di Trapani, D. Caironi, G. Valiulis, A. Dubietis, R. Danielius, and A. Piskarskas, "Observation of temporal solitons in second-harmonic generation with tilted pulses," *Phys. Rev. Lett.* **81**, 570-573 (1998).
29. N. Fujioka, S. Ashihara, H. Ono, T. Shimura, and K. Kuroda, "Group-velocity-matched noncollinear second-harmonic generation in quasi-phase matching," *J. Opt. Soc. Am. B* **22**, 1283-1289 (2005).
30. A. Schober, M. Charbonneau-Lefort, and M. Fejer, "Broadband quasi-phase-matched second-harmonic generation of ultrashort optical pulses with spectral angular dispersion," *J. Opt. Soc. Am. B* **22**, 1699-1713 (2005).
31. D. H. Jundt, "Temperature-dependent Sellmeier equation for the index of refraction, n_e , in congruent lithium niobate," *Opt. Lett.* **22**, 1553-1555 (1997).
32. J. C. Diels and W. Rudolph, *Ultrashort Laser Pulse Phenomena* (Academic, New York, 1996).
33. M. Marangoni, C. Manzoni, R. Ramponi, G. Cerullo, F. Baronio, C. De Angelis, and K. Kitamura, "Group-velocity control by quadratic nonlinear interactions," *Opt. Lett.* **31**, 534-536 (2006).
34. S. Carrasco, J. Torres, L. Torner, and F. W. Wise, "Walk-off acceptance for quadratic soliton generation," *Opt. Comm.* **191**, 363-370 (2001).

1. Introduction

Quadratic solitons, which are formed by mutual trapping of multiple-frequency components through cascaded quadratic nonlinearities, have been studied extensively because of their unique physical properties [1-4]. Typical geometry is the phase-mismatched second-harmonic generation (SHG), where the phases and the amplitudes of fundamental (FF) and second-harmonic (SH) waves are modulated through the continuous exchange of the energy between them. Families of quadratic soliton exist and are stable at various phase mismatch values [5-6]. The energy ratio of FF and SH waves as well as their beam widths are dependent on the phase mismatch and the total energy that they carry. Quadratic solitons in the space domain have been demonstrated in birefringently phase-matched crystals [7, 8] and in quasi-phase-matching (QPM) devices, such as periodically poled lithium niobate (PPLN) [9] and periodically poled KTiOPO₄ (PPKTP) [10]. Torner et al. [11] proposed the idea to

adiabatically shape the quadratic solitons to different beam profiles and widths or different fractions of energy carried by the SH wave. The shaping mechanism is based on soliton generation and propagation in chirped QPM gratings. The main advantage of this adiabatic shaping approach is that most of the energy incident as fundamental wave remains contained inside the two-color solitons. Carrasco et al. [12] theoretically showed that the efficiency and the mismatch bandwidth of quadratic soliton formation can be enhanced in synthetic phase-mismatching profiles. Excitation of spatial soliton families has been demonstrated in an engineered QPM lithium niobate waveguide so far [13].

Although the governing equations for spatial solitons and temporal solitons are similar, the realization of temporal solitons or soliton pulse compression is not straightforward. The main obstacle is the group-velocity (GV) mismatch between FF and SH, which is usually encountered in the experiment. The GV mismatch tends to distort the cascaded nonlinearities and prevent the pulses from forming solitons. One way to avoid the phase distortions is to operate the cascaded nonlinearities under large phase-mismatch condition, where the back-conversion length is less than the GV-mismatch length [14]. By using the self-defocusing nonlinearity at the large phase mismatch in beta-barium borate (BBO) and the material normal dispersion, pulse compression of fundamental pulses, centered at 800 nm, was demonstrated [15, 16]. The non-instantaneous feature of the cascading nonlinear phase shifts, caused by GV mismatch, has been highlighted as Raman-like nonlinearities [17]. It is shown that the Raman-like nonlinearities work for frequency shift and such shift is enhanced by the local control of the cascaded nonlinearities. Here the chirped QPM grating was used to keep the net phase mismatch constant along propagation and to avoid the saturation of the frequency shift. Recently, significant improvement has been made to this type of cascading pulse compressor: fundamental pulses are compressed down to few-cycle (12 fs) [18].

Large phase mismatch approach reduces the phase distortions, but it does so at the expense of nonlinearity. Moreover, the energy content in SH pulse is limited to be small. In contrast, GV matching between the interacting waves, if it is possible, allows us to operate the cascaded nonlinearities under small phase-mismatch condition without severe phase distortions. Therefore the cascaded nonlinearities of ultrashort pulses can be significantly enhanced and multi-color temporal solitons can be generated. The multicolored nature is one of the unique features of quadratic solitons. Simultaneously compressed FF and SH pulses of 35fs duration have been generated through GV matched cascaded quadratic nonlinearities [19]. Here type-I SHG geometry (e: $o + o$) in 10-mm MgO-doped periodically poled lithium niobate (PPMgLN) was used to achieve GV matching. The compression mechanism is based on the interplay between amplitude/phase modulation due to cascaded nonlinearities and the material dispersion of the PPMgLN. This non-adiabatic process is inherently accompanied by the large pedestals in the compressed pulses.

In this paper, we show that the pulse quality of the compressed FF and SH pulses can be significantly improved by adiabatically exciting the solitons in the chirped QPM gratings. We present the experimentally realistic setup for the adiabatic compression of two-colored pulses and confirm its performance by numerical simulations. Two different GV-matching (or GV-mismatch compensation) schemes available in QPM devices are exploited to implement the adiabatic compression at the fundamental wavelength of 1560 nm. One scheme involves achieving GV matching by using an off-diagonal nonlinear coefficient d_{32} (Type-I: e: $o + o$) in PPMgLN [20]. In the other scheme, the intrinsic GV mismatch is compensated for by using pulse-front tilting and noncollinear QPM (Type-0: e: $e + e$) [21]. In contrast to ref. [17], chirped QPM grating is used to let temporal solitons adiabatically adapt themselves to the local wave-vector mismatch in this paper. We compare pulse compression performance between two different GV-matching schemes and show their capabilities and limitations from a practical standpoint. The demonstrated two-colored soliton consists of FF and SH pulses, which are inherently pedestal-free and mutually trapped in time. These properties can be beneficial for applications in optical information processing or in light-matter control. Different from the pulse compression achieved by using large phase-mismatch [15-18], the GV-matched adiabatic scheme generates relatively large amount of SH energy. This points to

the application as an efficient SHG, where the compressed SH pulses with high quality factor are generated.

This paper is organized as follows. The concept of adiabatic soliton compression in QPM gratings is described in Sec. 2. Numerical results of the soliton compression based on the linearly chirped poled MgO-doped LiNbO₃ (MgO: LN) geometry (Type-I) are presented in Sec. 3. Numerical results of another GV-mismatch compensation based on the noncollinear QPM (Type-0) geometry are presented in Sec. 4. In Sec.5, we study the tolerance of adiabatic shaping to GV mismatch: the generation of quadratic walking solitons under the small GV mismatch condition is discussed. Here we observe deceleration or acceleration of quadratic walking solitons. Finally, we conclude this paper in Sec. 6.

2. Adiabatic soliton compression in QPM grating

The adiabatic compression technique was first presented in dispersion-decreasing optical fibers [22]. The fundamental soliton is maintained by the interplay between self-phase modulation (SPM) and anomalous group velocity dispersion (GVD). If this balance is perturbed by slowly decreasing the GVD of the fiber along the propagation direction, the soliton does not break down and adiabatically adjusts its pulse width owing to its stability. Then, the maximum compression factor is determined by the ratio of input to output GVD.

Quadratic solitons exist at different values of wave-vector mismatch, but their properties (energy ratio and shapes of FF and SH) are significantly different depending on the mismatch and the total energy. Chirped QPM yields the longitudinally varying wave-vector mismatch. If pulses are launched into the chirped QPM, the solitons adapt themselves adiabatically to the local wave-vector mismatch [11]. This ability originates from the stability, which is one of the fascinating properties of quadratic solitons. In fact, dynamic evolution of quadratic solitons can tolerate weak perturbations of the QPM period [23]. If we design the longitudinal distribution of the wave-vector mismatch properly, the SH pulses carry more energy and both FF and SH pulses have shorter pulse duration at the exit of the device, compared with the pulse duration at the entrance.

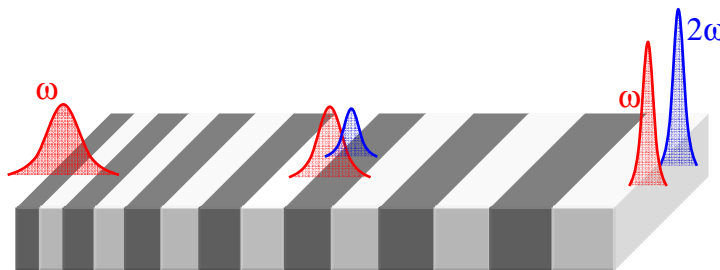


Fig. 1. Schematic of adiabatic compression process in the aperiodic QPM grating. The effective wave-vector mismatch $\Delta k(z)=k_2-2k_1-2\pi/\Lambda(z)$ varies along the propagation direction.

A simple schematic diagram of adiabatic compression is shown in Fig. 1. The effective wave-vector mismatch between FF and SH waves, $\Delta k(z)=k_2-2k_1-2\pi/\Lambda(z)$, is determined by the local domain reversal period $\Lambda(z)$ and the FF and SH wave numbers, k_1 and k_2 . Here, we consider a chirped QPM grating, where the local effective wave-vector mismatch longitudinally changes and approaches the phase matching condition. FF and SH pulses will dynamically adapt themselves to the soliton solutions for the local wave-vector mismatch. The local wave-vector mismatch should change slowly enough that pulses can adiabatically evolve to proper solitons at each position. Finally, both FF and SH pulses adiabatically evolve into soliton pulses with shorter pulse durations.

3. Soliton compression based on collinear QPM geometry

Owing to the unique material dispersion of 5 mol% MgO: LN, GV matching for SHG in the type-I geometry (e: $o + o$) occurs at the fundamental wavelength of 1560 nm [20]. We

investigate adiabatic soliton compression, which can be implemented in the type-I SHG geometry in the continuously chirped QPM grating. The QPM period $\Lambda(z)$ used in our simulation varies from 19.98 μm to 20.40 μm (Δk : 8.15 mm^{-1} to 0.41 mm^{-1}) with a simple linear chirp (see Fig. 2). The grating length is 100 mm, which corresponds to 3.3 times the dispersion length of a 100-fs pulse (FF). The coupled wave equations governing the propagation of the FF and SH waves under the slowly varying envelope approximation can be generalized as [24]:

$$\begin{aligned} \partial_z E_1 + i(k_1''/2)\partial_t^2 E_1 &= i\rho_1(z)E_1^*E_2 \exp(i\Delta k_0 z) + i\sigma_1 \left[|E_1|^2 E_1 + 2|E_2|^2 E_1 \right] \\ \partial_z E_2 + i(k_2''/2)\partial_t^2 E_2 &= i\rho_2(z)E_1E_1 \exp(-i\Delta k_0 z) + i\sigma_2 \left[|E_2|^2 E_2 + 2|E_1|^2 E_2 \right] \end{aligned} \quad (1)$$

where $\rho_i(z) = \omega d_{32}d(z)/cn_i$ and $\sigma_i = 3\omega_i\chi^{(3)}/8cn_i$. $E_i(z, t)$ denotes the amplitude of the electric field, and the subscripts 1 and 2 correspond to FF and SH pulses, respectively. Time t is measured in a frame of reference along with FF propagation. Group velocity dispersion $k_i'' = d^2k_i/d^2\omega$ and the material wave-vector mismatch $\Delta k_0 = k_2 - 2k_1$ are derived from Sellmeier's equation for MgO: LN [25]. It is noted that $d(z)$ is the normalized distribution of second-order nonlinearity along the aperiodic QPM grating. The input FF is a transform-limited pulse with a full-width at half-maximum (FWHM) duration of 100 fs (peak intensity: 20 GW/cm^2) at the wavelength of 1560 nm. Numerical simulation is carried out to solve Eq. (1) with a symmetric split-step beam-propagation method (BPM).

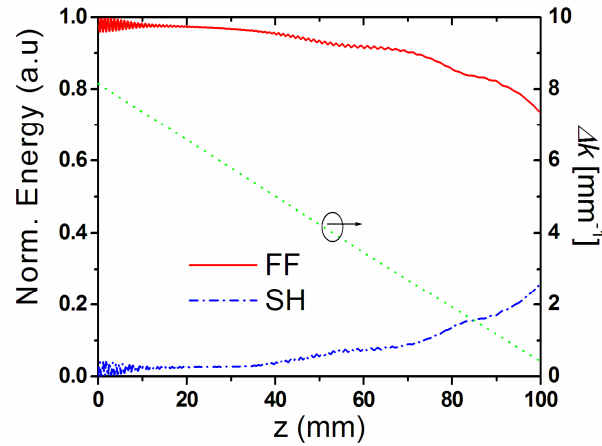


Fig. 2. Normalized energy ratio of FF and SH along the linearly chirped QPM grating. The effective wave-vector mismatch $\Delta k(z)$ varies from 8.15 mm^{-1} to 0.41 mm^{-1} . Input FF: transform-limited pulse (100 fs, 20 GW/cm^2) at the wavelength of 1560 nm;

The energy carried by the FF pulse is gradually transferred to the SH pulse, as shown in Fig. 2. What is usually encountered in experiments is that only FF pulse is input. The total energy is dominated by FF at the large wave-vector mismatch in the quadratic solitons. If larger wave-vector mismatch at the input is used, the launched FF pulse can be easily transformed to the quadratic soliton solution. After a rather short transition period of less than 10 mm (see Fig. 2), the oscillating energy exchange stops, and two-color solitons are formed. The mechanism of adiabatic soliton compression in chirped QPM grating is to allow quadratic solitons to adapt themselves to soliton families at the local wave mismatch [11]. The temporal profiles and energy fractions of output FF and SH are determined by the local effective wave-vector mismatch at the end of grating.

Figures 3(a)-3(b) show the intensity and phase profiles of input and output compressed FF and SH pulses in the chirped QPM grating. Here we see that the compressed temporal profiles show high-quality soliton-like shapes without obvious pedestals. Both FF and SH pulses are compressed to about 35 fs. The evolutions of the FF and SH pulse duration in the linearly chirped are plotted in Fig. 3(c). In adiabatic pulse shaping, the pulses tend to approach the solitary wave solutions, depending on the net nonlinearity including cascaded and cubic (third-order) nonlinearity at each position. Therefore the shortest pulse duration is determined by the input energy and the magnitude of nonlinearity. According to the numerical simulations including the cubic nonlinearity, the compressed pulse duration is 35 fs for the input fundamental pulses of 100 fs duration (peak intensity: 20 GW/cm²), as shown in Fig. 3. If we neglect the cubic nonlinear term, the compressed pulse duration becomes 25 fs. This means that the cubic nonlinearity counteracts the cascading self-defocusing nonlinearity and reduces the net nonlinearity. This trend becomes enhanced at higher intensity, because cascaded nonlinearity saturates with intensity. In fact, even if we increase the input peak intensity to be much more than 20 GW/cm², the compressed pulse duration decreases only down to 30 fs. Therefore, the shortest pulse duration is ~30 fs, mainly limited by the competition between cascaded second-order and cubic nonlinearity.

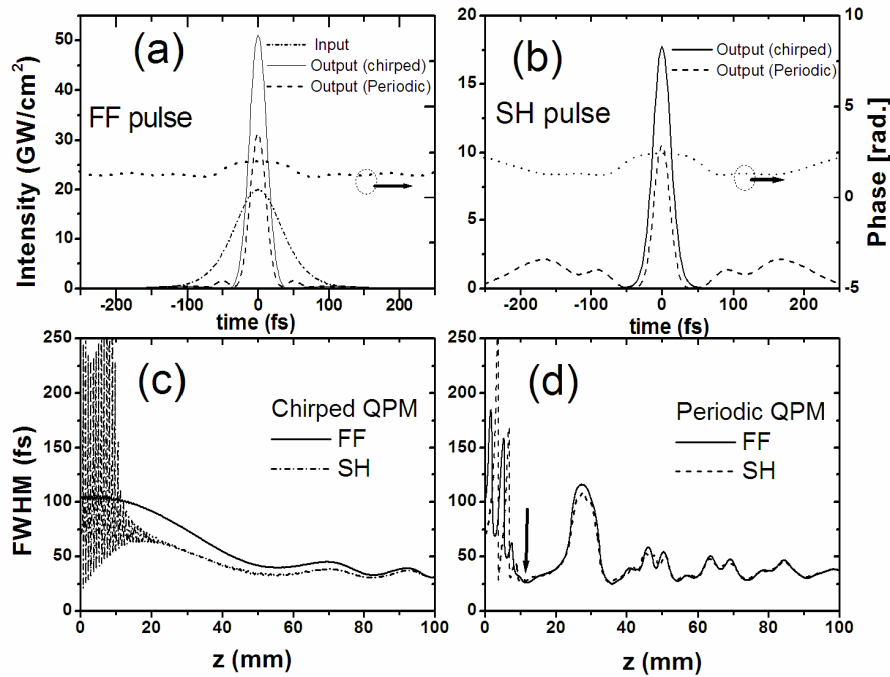


Fig. 3. Intensity profiles of the compressed (a) FF and (b) SH pulses in linearly chirped grating (100 mm, solid line) and periodic grating (10 mm, dashed line) at $\Delta k = 0.35 \text{ mm}^{-1}$. Phase profiles of the compressed (a) FF and (b) SH pulses for linearly chirped grating are also shown, as well as evolution of the pulse duration of the FF and SH pulses for (c) linearly chirped and (d) periodic QPM gratings.

Soliton compression in the periodic QPM structure is also investigated for comparison. It is numerically proved that at smaller (larger) Δk , the compressed pulses have shorter (longer) pulse duration with larger (smaller) pedestal. The effective wave-vector mismatch Δk is set to be 0.35 mm^{-1} for periodic QPM grating, which gives the same compression factor as the

adiabatic scheme. Then we can compare the performance as a compressor by the difference in pulse quality. Here self-defocusing nonlinearity is induced by the cascaded processes. The optimum propagation length (10 mm) for the maximum compression factor is taken after the initial compress stage, which is denoted by a black arrow in Fig. 3(d). After initial compress stage, FF and SH have same dynamic behavior. From the results in Figs. 3(a)-3(b), the output FF and SH pulses are compressed by a factor of about 3, but the pulse quality is degraded: the main spike is accompanied by a broad pedestal in both FF and SH pulses. From Fig. 3(d), FF and SH pulses experience several stretch and compression phases during the initial compression stage.

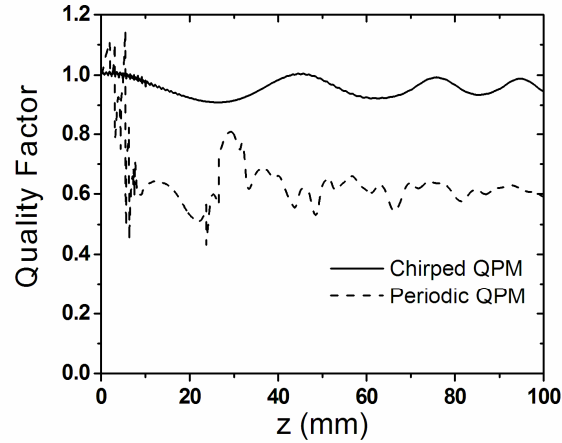


Fig. 4. Quality factors of the linearly chirped and periodic QPM gratings as a function of propagation length

We also evaluate the quality of the compressed pulses. The pulse shapes of quadratic solitons are different along the effective wave-vector mismatch Δk , but they are very close to the hyperbolic-secant or Gaussian functions. In simple terms, a $\text{sech}^2(t)$ function is used to fit the central part of the FF and SH pulses at each position. In this paper, the term quality factor is defined as the fractional amount of energy carried by the central spike of the FF and SH pulses, normalized by the launched energy. Figure 4 shows the quality factor as a function of propagation distance in the linearly chirped QPM grating (solid line). We can see that the quality factor is around 1 during propagation. This means that two-color (FF and SH) solitons show strong robustness and adapt to slight variations of Δk by reshaping their profiles. We note that the quality factor is larger than 1 at several regions due to mathematical artifacts, i.e., an intensity profile having a super-Gaussian shape will produce a quality factor larger than 1. Figs. 5(a)-5(b) show the evolutions of FF and SH pulses in the linearly chirped 100-mm QPM grating. No obvious energy leakage is visible. In contrast, the quality factor becomes as low as 0.6 in the periodic QPM grating (dash line in Fig. 4). The main lobe of FF and SH splits into a multi-peaked structure and a large part of the launched energy flows away in the form of a broad continuum, as shown in Figs. 5(c)-5(d).

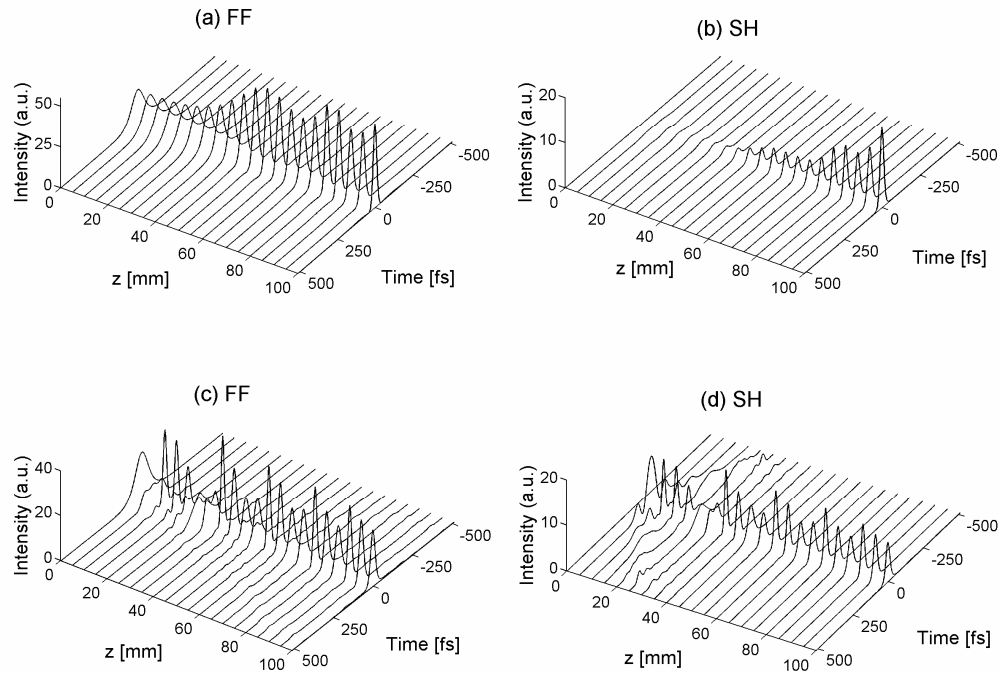


Fig. 5. Evolution of FF and SH pulses. (a) FF and (b) SH pulses in linearly chirped QPM; (c) FF and (d) SH pulses in periodic QPM at $\Delta k = 0.35 \text{ mm}^{-1}$.

From the discussions above, non-adiabatic compression in periodic QPM grating shows stronger compression ability than adiabatic soliton compression. However, the outstanding advantages of adiabatic soliton compression are (1) good quality of compressed pulses, (2) relatively large amount of energy in SH, (3) well-controlled timing (or time-coincidence) between the output FF and SH pulses. If one is interested in SH pulses, the adiabatic process can be seen as high-efficiency SHG process, accompanied by pulse compression. The timing-locked two-colored pulses may have new applications in optical information processing or in light-matter control. This approach is straightforward to implement pulse compression and can be extended in the waveguide structure, which is a promising application for pulse compression of mode-locked erbium-glass lasers.

4. Soliton compression in noncollinear QPM geometry

Achromatic phase-matching (APM) for SHG in birefringently phase-matched crystals [27] can compensate for GV mismatch between the FF and SH waves. This technique was utilized for the formation of $\chi^{(2)}$ temporal solitons in BBO crystal [28]. In addition, use of the APM technique for SHG based on QPM was proposed [21] and experimentally demonstrated [29, 30]. We will apply this scheme to achieving adiabatic soliton compression in the chirped QPM grating.

Let us first review GV-mismatch compensation in a noncollinear SHG geometry. The configuration is almost the same as that shown in Fig. 6(a) except that periodic QPM grating is used for a simple SHG. If spectral angular dispersion is properly introduced to the FF and SH waves, different spectral components propagate at their phase matching angles and the SHG bandwidth is broadened. This is equivalent to canceling the GV mismatch in the time domain. Spectral angular dispersion manifests itself as pulse-front tilting. When an appropriate angle of pulse-front tilting is introduced, the pulse fronts of the FF and SH waves

remain overlapped and in parallel as they propagate in the time domain; that is, the components of group velocities normal to the pulse front have the same velocity. The effective GV mismatch is also controllable by detuning from the GV-mismatch compensation condition.

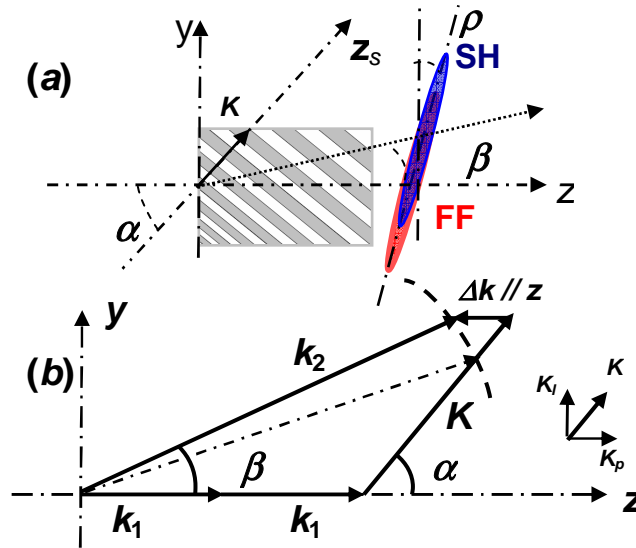


Fig. 6. (a). Schematic of SHG interactions in aperiodic noncollinear QPM grating and (b) the corresponding wave-vector diagram; $\Delta \mathbf{k} = k_{2z} - 2k_{1z} - K_p$ is the effective wave-vector mismatch; α , β and ρ are the propagation angle with respect to the grating vector \mathbf{K} , the walk off angle, and the pulse front tilt angle ρ .

Here congruent lithium niobate is considered for the type-0 ($e: e + e$) QPM gratings, and the material parameters are taken from Sellmeier's equation [31]. Under the condition of quasi-phase matching in the noncollinear QPM geometry, the walk-off angle β depends on the QPM grating vector $\mathbf{K} = 2\pi/\Lambda$, which is always longer than grating vector in collinear QPM grating, i.e. $\Lambda < \Lambda_0$. That is, the walk-off angle β (or the QPM period Λ) is a free parameter in the noncollinear QPM geometry. We express this freedom by a parameter $R = \Lambda/\Lambda_0$ ($0 < R < 1$), where Λ_0 is the QPM period of the collinear geometry. Once R is chosen, (1) the propagation angle α with respect to the grating vector \mathbf{K} and the walk-off angle β are determined to satisfy the noncollinear QPM condition, and (2) the pulse-front tilt angle ρ is determined for GV mismatch compensation. For example, when R is 0.3 ($\Lambda = 5.61 \mu\text{m}$), the achromatic QPM condition at the fundamental wavelength of 1560 nm requires α , β , and ρ to be 74.3° , 3.5° and 36.5° , respectively. FF is required to have a suitable pulse-front tilt before entering the QPM grating and the suitable spectral angular dispersion is necessary to compensate for the pulse-front tilt of output FF and SH, respectively.

Based on this knowledge, let us investigate adiabatic soliton compression based on the scheme of GV mismatch compensation, except chirped noncollinear QPM grating is used, as shown in Fig 6(a). The grating period is chirped along the direction of the grating vector \mathbf{K} , while the propagation angle α is same with that (74.3°) in the periodic noncollinear QPM grating. The value of grating vector \mathbf{K} is determined by the grating period along the coordinate z_s ($z_s // \mathbf{K}$), which has same period with the grating period along the line $z_s = y \sin(\alpha) + z \cos(\alpha)$ in (y, z) coordinates. That is, grating vector \mathbf{K} along this line is determined by $\mathbf{K}(z_s)$. Therefore the grating vector $\mathbf{K}(y, z)$ can be expressed as two components $[K_l(z_s), K_p(z_s)]$ in (y, z) coordinates. The first-order Fourier component of the nonlinear coefficient distribution is expressed as $d(z, y) = 2/\pi d_{33} \exp [iK_p \cdot z + iK_l \cdot y]$. The wave-vector diagram of noncollinear

SHG is shown in Fig. 6(b). The effective wave-vector mismatch $\Delta k(z) = k_{2z} - 2k_1 - K_p$ is parallel to the z direction, where k_{2z} and k_{2y} represent the z and y components of k_2 . $\Delta k(z)$ is designed to vary linearly from -40 mm^{-1} to 5 mm^{-1} . Strictly speaking, GV mismatch compensation becomes imperfect as we introduce effective wave-vector mismatch. Such degradation of the GV-mismatch compensation, however, is too small to affect the nonlinear propagation, and therefore is not taken into account here.

The coupled-wave equations governing the propagation of FF and SH in a noncollinear QPM configuration are given by [29]:

$$\begin{aligned} L_1 E_1 &= -i\rho_1 E_1^* E_2 \exp(i\Delta k z) - i\sigma_1 \left[|E_1|^2 E_1 + 2|E_2|^2 E_1 \right] \\ L_2 E_2 &= -\delta \cdot \partial_z E_2 - \eta \cdot \partial_y E_2 - i\rho_2 E_1 E_1 \exp(-i\Delta k z) - i\sigma_2 \left[|E_2|^2 E_2 + 2|E_1|^2 E_2 \right] \end{aligned} \quad (2)$$

where $L_i = \partial_z + \left[(2k_i)^{-1} \partial_{yy}^2 - (k_i^*/2) \partial_{zz}^2 \right]$, $\rho_i = 2\omega_i d_{33} / \pi c n_i$, $\delta = 1/v_{g1} - 1/v_{g2}$ is temporal walk-off, v_{g1} and v_{g2} are the group velocities of the FF and SH pulses, and $\eta = k_{2y}/k_{2z}$. The standard (2 + 1)D (temporal, spatial plus propagation) coupled-wave equations are solved by using the 2D BPM method.

The input FF pulse is transform-limited to 100-fs (FWHM) duration and 500- μm (FWHM) beam width, and the peak intensity is $20 \text{ GW}/\text{cm}^2$. The grating length L is set to be 3 mm, which is 3 times the effective dispersion length of the 100-fs duration pulse (FF). The effective GVD induced by the pulse-front tilting is given by [32]:

$$GVD_{eff} = -\lambda^3 \left(\frac{d\alpha}{d\lambda} \right)^2 (2\pi c^2)^{-2}, \quad (3)$$

where c is the velocity of light in vacuum and $d\alpha/d\lambda$ is the spectral angular dispersion. The effective GVD is usually one order of magnitude larger than the intrinsic material GVD. Different from the type-I case, the self-focusing nonlinearity works for soliton formation, because the net dispersion is anomalous: the net dispersion is mainly governed by the anomalous dispersion induced by pulse-front tilt. Therefore the cubic nonlinearity supports the cascading (self-focusing) nonlinearity to work for compression. In principle, the compression factor increases with intensity. For example, the compressed pulse duration becomes 25 fs when the input peak intensity is $40 \text{ GW}/\text{cm}^2$. However, the material damage threshold limits the highest input intensity.

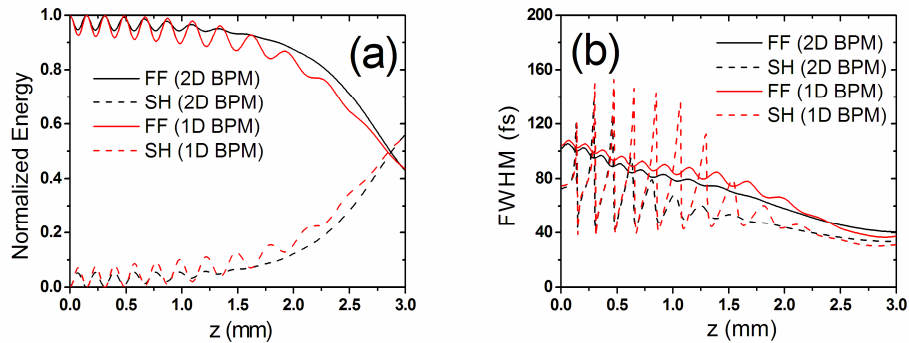


Fig. 7. Evolution of (a) normalized energy ratio and (b) pulse duration of FF (solid line) and SH (dashed line) pulses in the noncollinear QPM geometry from the results of 2D BPM (black lines) and 1D BPM (red lines). The effective wave-vector mismatch Δk_z of the engineered QPM grating varies from -40 mm^{-1} to 5 mm^{-1} with a linear variation ($R = 0.3$).

Figures 7(a)-7(b) show typical results, which illustrate adiabatic compression process of the tilted pulses (black lines). Durations of the FF and SH pulses gradually decrease, and the SH pulse carries more energy as it propagates. The sets of numerical simulation confirm that 3 mm grating length is long enough to achieve adiabatic soliton compression. It is noted that SH carries more energy than FF. Figure 8(a) shows temporal profiles at the spatial centre of the FF and SH pulses. The compressed FF (40 fs) and SH (35 fs) pulses are obtained without observable pedestals. The large effective anomalous GVD is responsible for the effectiveness of the shorter length in the noncollinear QPM grating, compared with the type-I QPM geometry (100 mm) in section 4. The larger nonlinear coefficient d_{33} used in the type-0 phase matching geometry makes the cascaded nonlinearity more efficient for soliton compression.

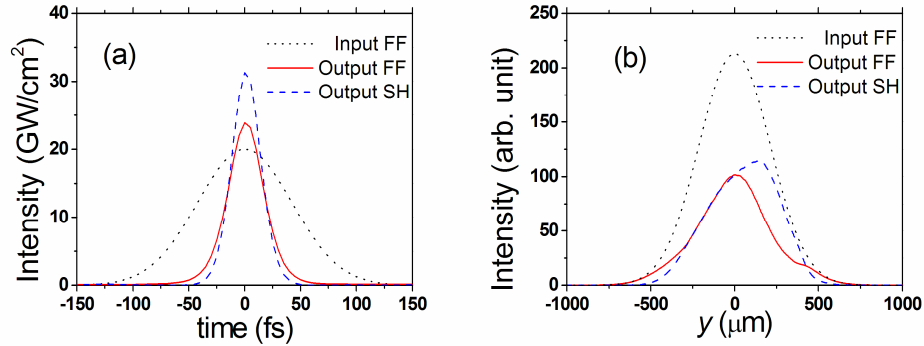


Fig. 8. (a). Temporal profiles at the spatial centre and (b) time-integrated spatial profiles of FF (solid-black line) and SH (dashed-red line) pulses. Dotted-green lines indicate the input profiles.

Figure 8(b) shows the time-integrated spatial profiles of the FF and SH pulses. The compressed pulses are pedestal-free obviously. Small asymmetry in the FF and SH spatial profiles is shown due to the spatial walk-off. The separation between FF and SH pulses can be characterized by the aperture length in the lateral direction, which is denoted as $D = \beta L$. The aperture length D is $180 \mu\text{m}$ after 3 mm propagation, which is much less than the $500 \mu\text{m}$ (FWHM) beam width. It is pointed out that spatial walk-off in the noncollinear interaction has less influence on the pulse compression if large-diameter beams are used. This means that spatial walk-off does not degrade the interaction between FF and SH pulses. To verify this point, we investigate the temporal behaviors without considering the spatial walk-off. The equations for this case are similar to Eq. (1) except that the GVD coefficients of FF and SH are modified by the effective anomalous GVD, which is induced by the pulse-front tilting. The normalized energy ratio and pulse duration of the FF and SH pulses are calculated by using a 1D BPM method (red lines), as shown in Figs. 7(a)-7(b) for comparison. The agreement between the results for 1D and 2D simulations is clearly shown, which demonstrates that spatial walk-off has little influence on the pulse compression.

We conclude that a short grating length (3 mm) is sufficient to achieve adiabatic soliton compression in the scheme of GV-mismatch compensation based on the noncollinear aperiodic QPM geometry. The effect of spatial walk-off on the pulse compression is negligible if a beam larger than the aperture length is used. As compared with adiabatic soliton compression in type-I geometry, (1) the largest nonlinear coefficient d_{33} (Type-0: $e: e + e$) can be used in this scheme; (2) Shorter gratings become available in noncollinear QPM grating due to the induced effective GVD from pulse-front tilting. Since GV-mismatching compensation in other wavelengths can be achieved in non-collinear QPM gratings, adiabatic soliton compression can be applied to a broad FF wavelength. This approach shows an efficient way to achieve adiabatic soliton compression in the bulk $\chi^{(2)}$ media.

5. Adiabatic soliton compression under small GV mismatch

It is also interesting to study the adiabatic process under small, but non-zero, GV-mismatch. It is known that in the presence of GV mismatch, FF and SH pulses mutually trap and drag each other and propagate with a velocity between the non-interacting FF and SH group velocities. The velocity of walking solitons is determined by the energy distribution between FF and SH pulses. GV control of ultrafast pulses was demonstrated through $\chi^{(2)}$ cascaded interactions in QPM gratings [33]. The soliton content, or soliton generation efficiency, decreases as the phase mismatch decreases (or larger walk-off between FF and SH) when only FF is input in periodic QPM grating (i.e. non-adiabatic process) [34]. In the following simulations, we find that the adiabatic process in the chirped QPM grating can tolerate small GV mismatch.

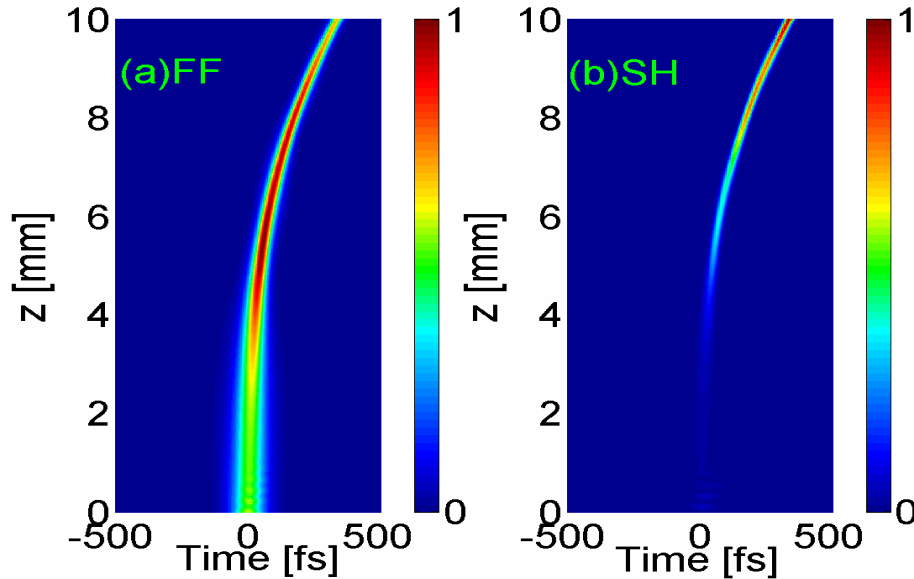


Fig. 9. Evolutions of normalized intensity profiles of (a) FF and (b) SH pulses in the presence of GV mismatch ($\delta=0.025$).

Walking solitons in the noncollinear type-0 QPM scheme are investigated. The effective GV mismatch is controlled by slightly detuning from the effective GV-matching condition. The grating length is chosen to be 10 mm in order to show clearly the change in the group velocity with propagation. Here δ is the GV mismatch normalized with the group velocity of the FF pulse. The normalized GV mismatch δ is positive if the effective GV of the FF pulse is smaller than that of the SH pulse.

Figures 9(a)-9(b) show that walking solitons including FF and SH fields propagate with modified walking velocities relative to the non-interacting FF group velocity. The walking solitons decelerate with propagation because the energy carried by the SH pulse increases with propagation. Moreover, walking solitons can gradually accelerate if the effective GV mismatch $\delta < 0$.

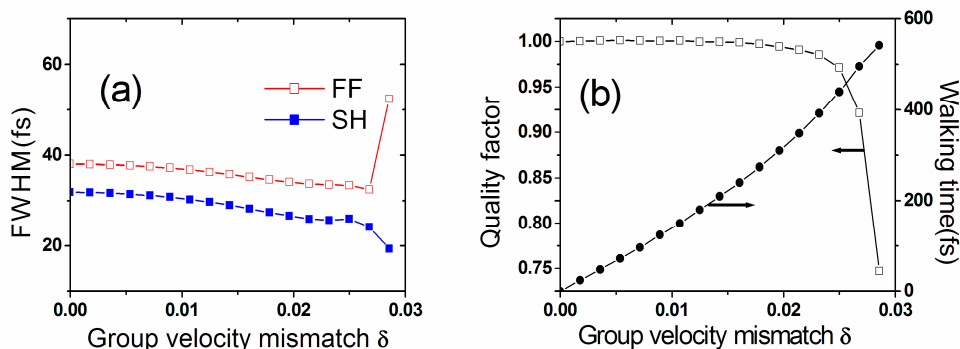


Fig. 10. Dependence of (a) FWHM of FF and SH and (b) quality factor and walking time on the normalized group velocity mismatch δ .

Figure 10(a) shows the dependence of the FWHM of FF and SH pulses on the normalized GV mismatch δ , and Fig. 10(b) shows the dependence of the quality factor and walking time on the normalized GV mismatch δ after 10 mm propagation. Here the walking time is defined as the temporal delay of the quadratic solitons relative to the reference frame of the non-interacting FF group velocity. FF and SH pulses less than 40 fs in width are also compressed within $\delta < 0.025$, while maintaining a high quality factor. If δ is larger than that, the FF pulse broadens and the SH pulse breaks into multi-peaks. The peaks of quadratic solitons are temporally delayed, and significant walking times are induced.

These results clearly show that adiabatic soliton compression takes effect even in the presence of group velocity mismatch. The compression factor and quality factor are not degraded in the quadratic solitons under small GV mismatch ($\delta < 0.025$) conditions. Walking solitons can gradually decelerate (accelerate) according to the sign of the effective GV mismatch. In the way, group velocities of quadratic solitons are controlled by using aperiodic QPM gratings. Adiabatic process with a small GV mismatch may serve as GV control scheme.

6. Conclusions

We investigate the practical approach to achieve adiabatic soliton compression of femtosecond pulses based on GV-matching in aperiodic collinear (type-I) QPM and GV-mismatch compensation in noncollinear (type-0) QPM gratings. Quadratic temporal solitons with pulse duration less than 40 fs are generated without visible pedestals from 100-fs FF pulses at the center wavelength of 1560 nm. The demonstrated adiabatic pulse shaping schemes are very attractive because of their ability to efficiently generate two-color solitons with shorter pulse durations. These timing-locked two-colored pulses may have new applications in the optical information processing or in the light-matter control. Even in the presence of small GV mismatch, walking solitons are adiabatically compressed with the decelerated (accelerated) group velocities. These results point to the new application to the group-velocity control through adiabatic process.

7. Acknowledgments

This work is supported by JSPS (Japan Society for the Promotion of Science), MEXT KAKENHI (18686007), and research grants from the Asahi Glass Foundation. The authors thank M. Cha, N. E. Yu, and S. Kurimura for useful discussions. Xianglong Zeng's email address is zenglong@iis.u-tokyo.ac.jp.